

Creep Characterization of Aluminum-Magnesium Solid-Solution Alloy through Self-Similar Microindentation*¹

Hidehiko Takagi¹, Ming Dao², Masami Fujiwara¹ and Masahisa Otsuka^{3,*2}

¹Division of Applied Physics, College of Engineering, Nihon University, Fukushima 963-8642, Japan

²Department of Materials Science and Engineering, School of Engineering, Massachusetts Institute of Technology, Massachusetts 02139, USA

³Department of Materials Science and Engineering, Faculty of Engineering, Shibaura Institute of Technology, Tokyo 108-8548, Japan

Indentation creep tests were performed on an Al-5.3 mol% Mg solid-solution alloy to examine whether mechanical properties can be extracted accurately from a testpiece, as small as a rice grain. A conical diamond indenter was pressed into a test surface with a constant load F at temperatures ranging from 0.60 to 0.65 T_m (T_m : the absolute liquidus temperature). When the representative flow stress $\bar{\sigma}_m$ and the indentation strain rate $\dot{\epsilon}_{in}$ in the underlying material decreases to each critical value, $\bar{\sigma}_c$ and $\dot{\epsilon}_c$, as indentation creep proceeds, the stress exponent n for creep varies distinctively from 4.9 to 3.0. The measured $\bar{\sigma}_c$ decreases with increasing temperature, while the corresponding indentation strain rate $\dot{\epsilon}_c$ increases under the same condition. This temperature dependence is in close agreement with the results derived from the dislocation theory. The activation energy Q for creep in range M ($n \cong 5$, $\bar{\sigma}_m > \bar{\sigma}_c$ or $\dot{\epsilon}_{in} > \dot{\epsilon}_c$) is approximately equivalent to that for the lattice diffusion of pure aluminum, and the Q value in range A ($n \cong 3$, $\bar{\sigma}_m < \bar{\sigma}_c$ or $\dot{\epsilon}_{in} < \dot{\epsilon}_c$) is close to that for the mutual diffusion of this alloy. With load-jump tests, F was abruptly increased in the indentation creep test. In range M, instantaneous plastic deformation (IPD) takes place evidently even with a slight abrupt increase in load. On the other hand, the IPD does not occur in range A when load increment is within a certain value. However, the occurrence of IPD is observed under the condition of $\bar{\sigma}_m > \bar{\sigma}_c$ or $\dot{\epsilon}_{in} > \dot{\epsilon}_c$. The findings suggest that the creep rate-controlling process changes from the recovery control ($n \cong 5$) to the glide control ($n \cong 3$) below $\bar{\sigma}_c$. It is thus demonstrated that the indentation testing technique can be effectively used to extract material parameters equivalent to those obtained from conventional uniaxial creep tests in the dislocation creep regime. [doi:10.2320/matertrans.47.2006]

(Received March 15, 2006; Accepted June 30, 2006; Published August 15, 2006)

Keywords: aluminum-magnesium alloy, creep, indentation, self-similar indenter, load-jump test, stress exponent, activation energy, dragging viscous glide, rate-controlling process

1. Introduction

In general, it is often difficult to prepare many specimens for mechanical tests with advanced materials, *e.g.*, nano-materials, amorphous materials and quasicrystalline materials, which are often available only in minute quantities or as small-volume specimens or structures. It is very important to establish a robust and systematic material testing technique that can accurately extract mechanical properties at both ambient and high temperatures from small-volume specimens. How can we extract material parameters such as power-law creep exponents and activation energy for creep equivalent to those obtained from conventional uniaxial creep tests using a testpiece as small as a rice grain? The prerequisites to achieve such technical demands are as follows.

- Creep deformation does not depend on the size and shape of specimens.
- The parameter employed to describe the rate of creep deformation is proportional to the equivalent plastic strain rate.

Thus, it is necessary to develop a new testing machine that is designed to fulfill these two requirements and furthermore to derive a constitutive equation for analyzing the data measured with this testing machine.

The self-similar indentation test is one of the methods of

evaluating the high-temperature mechanical properties of a small-volume material. In the test, a conical indenter is pressed into the surface of a heated specimen with various load modes. At high temperatures, indenter displacement increases with indentation time. Both indentation load and indenter displacement are recorded simultaneously with time and analyzed to evaluate high-temperature mechanical properties. The time-dependent deformation in the underlying material is called indentation creep.

Considerable effort and significant progress have been made in extracting the ambient and high-temperature properties of materials using the indentation testing technique.^{1,2} Mulhearn and Tabor investigated the relationship between indentation hardness and loading time.³ Li *et al.* tried to analyze all deformation mechanisms that may contribute to indentation creep.⁴ Sargent and Ashby demonstrated that hot hardness tests provide information concerning the time-dependent flow, or creep, of the material beneath a self-similar indenter.⁵ Prakash proposed a conceptual model wherein the creep deformation just below a conical indenter can be interpreted to be in a steady state.⁶ Lucas and Oliver obtained the creep properties for materials of low melting point using a nanoindenter.⁷ Fujiwara and Otsuka derived a set of constitutive equations for self-similar indentation creep and carried out high-temperature indentation tests on pure metals, solid-solution alloys, dispersion-strengthened alloys, and two-phase alloys using a microindenter. Then, they reported that the measured creep properties agreed well with those obtained from conventional tensile-creep tests.⁸⁻¹⁰ Takagi *et al.*¹¹ and Dao *et al.*¹² performed finite-element

*¹This Paper was Originally Published in Japanese in J. Japan Inst. Metals **69** (2005) 348-355.

*²Passed away.

Table 1 Chemical composition of tested material.

Test material	Analysed composition (mol%)				
	Mg	Si	Fe	Cu	Al
Al-Mg alloy	5.3	0.004	0.004	0.0002	Balance

computations for indentation creep, and proved that the plastic region just below the indenter extends while maintaining its geometrical self-similarity as indentation creep proceeds.

In the present study, we conduct constant-load indentation tests and load-jump tests on an Al-5.3 mol% Mg alloy with a microindenter, and examine the following three aspects.

- The temperature dependence of critical stress level and indentation strain rate when the stress exponent n for creep varies distinctively from 5 to 3 as indentation creep proceeds.
- The predominant, and thus rate-controlling, creep process in each range of $n \cong 5$ and $n \cong 3$.
- The switching model of the rate-controlling process when some deformation mechanisms operate simultaneously in the underlying material.

Then, it is demonstrated that the self-similar indentation technique can be effectively used to extract material parameters equivalent to those obtained from conventional uniaxial creep tests in the dislocation creep regime, and that this testing technique is a powerful tool to evaluate mechanical properties from a testpiece as small as a rice grain.

2. Experimental Procedures

An ingot of Al-5.3 mol% Mg alloy was subjected to a homogenization treatment in argon gas for 86.4 ks at 773 K ($0.85 T_m$). Its chemical composition is shown in Table 1. The alloy was cut into 5 mm \times 10 mm \times 5 mm rectangular parallelepipeds with a metal saw and carefully shaped so that the test surface (5 mm \times 10 mm) became parallel to the bottom surface using special jigs and emery papers. All specimens were annealed in argon gas for 3.6 ks at 773 K. After that, they were electropolished to remove the surface layer of up to 40 μ m in thickness and immediately placed in the testing machine to minimize atmospheric tarnish. The electropolishing was carried out under a condition of 14.5 kA/m² for 900 s at 273 K. The polishing solution consists of 10 ml of perchloric acid, 20 ml of ethylene glycol and 400 ml of ethyl alcohol.

Figure 1(a) schematically shows the instrumented microindenter (ULVAC-RIKO, Inc., JAPAN) used in this study.⁸⁾ The conical indenter tip of diamond (the included apex angle: $2\theta = 136^\circ$) was pressed perpendicularly into the 5 mm \times 10 mm surface area of the heated specimen in an argon gas atmosphere. The indentation load was controlled by an electromagnet accurately, and the indentation depth was obtained by measuring the displacement of the indenter column with a linear variable-differential transformer (LVDT). The constant-load test conditions applied are as follows: indentation load, 0.39 N; test temperatures, 546–590 K ($0.60 T_m$ – $0.65 T_m$); total indentation time, 1200 s. Load-jump tests were performed at a temperature of 573 K, in

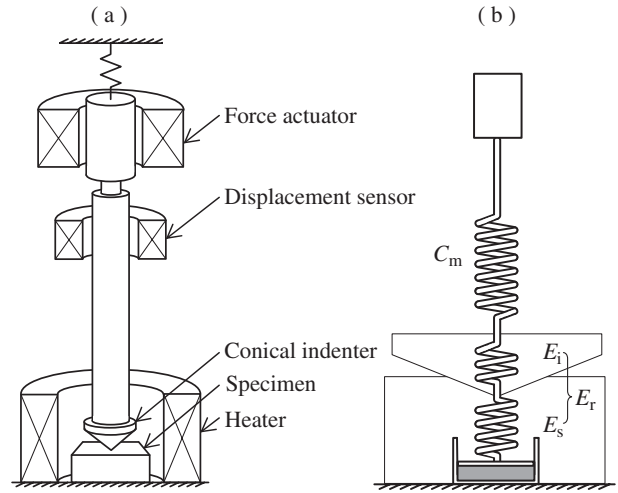


Fig. 1 (a) Schematic diagram and (b) dynamic mechanical model of a microindenter. C_m : compliance of testing machine, E_r : reduced elastic modulus, E_i : Young's modulus of indenter tip and E_s : Young's modulus of specimen.

which indentation load was abruptly changed from 0.39 N to 0.39 ± 0.20 N. The applied load could reach the desired value within less than 0.1 s. All the indentation tests were carried out after keeping at the test temperatures for 1800 s. The temperature variation during indentation creep tests was within ± 1 K.

3. Constitutive Equation of Indentation Creep

A set of constitutive equations for indentation creep has been derived by Fujiwara and Otsuka.⁸⁾ Its outline is described as follows. When a sharp indenter is pressed into the surface of a heated material, it penetrates with the rate-dependent and temperature-dependent yielding and creeping of the indented material. The time-dependent flow, or creep, of the material just below the indenter is called indentation creep. Using a self-similar sharp indenter (*e.g.*, cone or pyramid) under a constant load, it is often assumed that the plastic region beneath the indenter extends while maintaining its geometrical self-similarity under the equilibrium of forces as indentation creep proceeds; that is, the contour lines of plastic strain change only in scale, and not in shape.¹³⁾ Recently, this prerequisite has been carefully confirmed by Takagi *et al.* using finite-element calculations.¹¹⁾ The velocity of the indenter column, hereafter called indenter velocity, is governed by creep in a certain limited region beneath the indenter, which is called control volume (CV). When geometrical self-similarity holds for the distribution of plastic strain, the deformation rate $\dot{\epsilon}_{in}$ in the CV, hereafter called indentation strain rate, can be defined by

$$\dot{\epsilon}_{in} = \frac{\dot{u}}{u}, \quad (1)$$

where u is the indenter displacement and \dot{u} is the indenter velocity which is obtained from differentiating u with respect to indentation time.^{14,15)} For equilibrium after yielding, the representative stress $\bar{\sigma}_m$ in the CV can be approximately written as^{16–18)}

$$\bar{\sigma}_m \approx \frac{p}{3} = \frac{F}{3\pi u^2 \tan^2 \theta}, \quad (2)$$

where p is the indentation pressure, which is obtained by dividing the indentation load F by the projected contact area of an impression. The equivalent stress $\bar{\sigma}$ at an arbitrary point in the CV can be given as

$$\bar{\sigma} = C_1 p \propto \bar{\sigma}_m, \quad (3)$$

where C_1 is a dimensionless constant that depends on the position of interest. For compatibility, the equivalent plastic strain rate $\dot{\bar{\epsilon}}$ at that point is given as¹⁴⁾

$$\dot{\bar{\epsilon}} = C_2 \dot{\epsilon}_{in}. \quad (4)$$

Here, C_2 is a dimensionless constant of approximately 1/3 in isotropic materials. When creep deformation at the point is taken to be in a steady state, where dynamic recovery compensates strain hardening, it is assumed that $\dot{\bar{\epsilon}}$ can be described by the well-known power-law creep equation

$$\dot{\bar{\epsilon}} = A_1 \left(\frac{\bar{\sigma}}{E} \right)^n \exp\left(-\frac{Q}{RT}\right), \quad (5)$$

where A_1 is a material constant with the dimension of the reciprocal of time, E Young's modulus, R the gas constant, and T the test temperature. The power-law creep exponent n and the activation energy Q for creep are constants that are uniquely determined by the predominant rate-controlling process of creep deformation. By combining eqs. (1)–(5), a set of constitutive equations for indentation creep can be obtained as

$$\dot{u} = A_2 u \left(\frac{F}{Eu^2} \right)^n \exp\left(-\frac{Q}{RT}\right) \quad (6)$$

or

$$\dot{\epsilon}_{in} = A_3 \left(\frac{\bar{\sigma}_m}{E} \right)^n \exp\left(-\frac{Q}{RT}\right), \quad (7)$$

where A_2 and A_3 are constants with the dimension of the reciprocal of time. From eq. (7), the stress exponent n for creep can be given by

$$n = \left[\frac{\partial \ln \dot{\epsilon}_{in}}{\partial \ln (\bar{\sigma}_m/E)} \right]_T. \quad (8)$$

From eq. (6), the activation energy Q for creep can be expressed as

$$Q = -R \left[\frac{\partial \ln K}{\partial (1/T)} \right], \quad (9)$$

where $K = \dot{u} u^{-1} (Eu^2/F)^n$. This variable has the dimension of the reciprocal of time, and it is named K -parameter hereafter.

4. Results

4.1 Constant-load indentation creep test

Figure 2 shows the indenter displacement u versus indentation time t plots. These are typical indentation creep curves (ICCs) obtained at each temperature. The measured u increases gradually with the passage of indentation time, following the instantaneous deformation occurring right after the application of load. The projected contact area of an

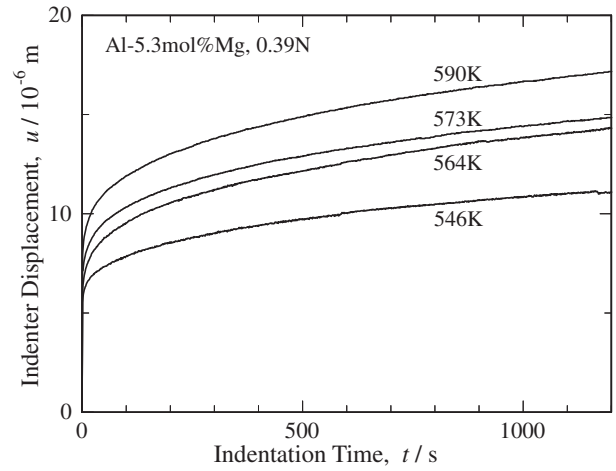


Fig. 2 ICCs of Al-5.3 mol%Mg solid-solution alloy measured with $F = 0.39$ N at $T = 546, 564, 573$ and 590 K.

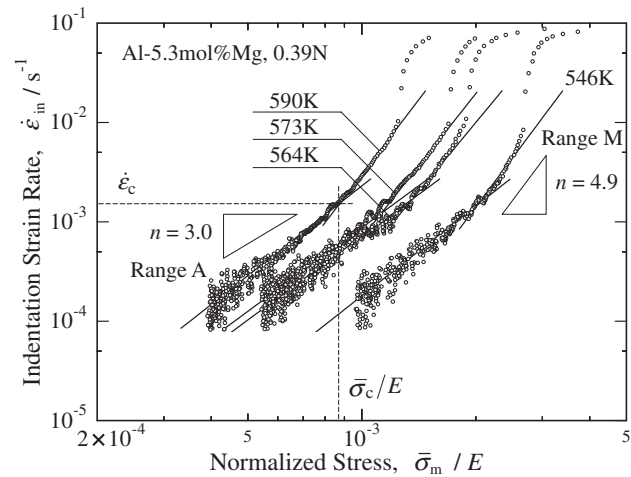
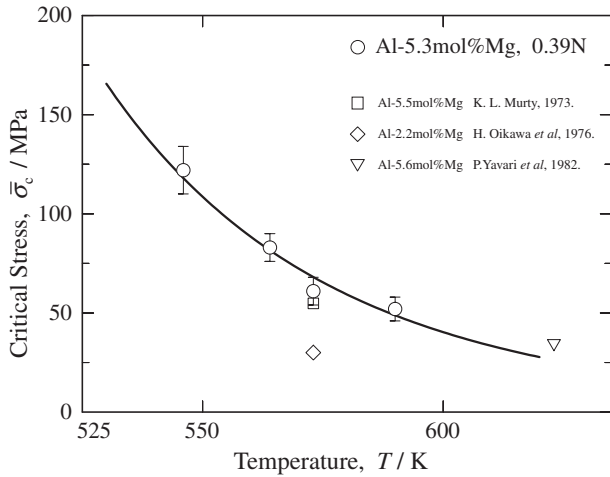
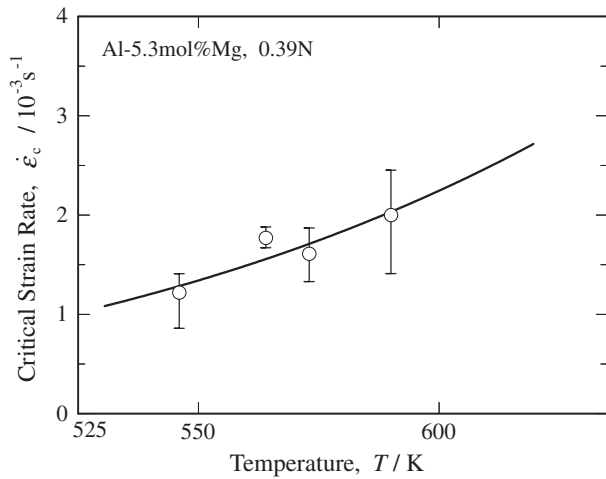


Fig. 3 Relationship of $\dot{\epsilon}_{in}$ versus $\bar{\sigma}_m/E$, both on logarithmic scales. The creep stress exponent n varies distinctively from 4.9 to 3.0 at the critical stress $\bar{\sigma}_c$ and the corresponding indentation strain rate $\dot{\epsilon}_c$.

impression increases as indentation creep proceeds. Correspondingly, the indentation pressure p and the representative stress $\bar{\sigma}_m$ in the underlying material uniformly decrease with indentation time. Also, the shape of the ICCs indicates that the indenter velocity \dot{u} and the indentation strain rate \dot{u}/u decrease gradually. In Fig. 3, the indentation strain rate $\dot{\epsilon}_{in}$, that is \dot{u}/u , is plotted against the representative stress normalized by Young's modulus¹⁹⁾ at each temperature, $\bar{\sigma}_m/E$. Note that the indentation creep proceeds from the high-stress range to the low-stress range. The experimental data lie on two straight lines with different slopes, except for the initial transient stage right after loading and the range beyond the measurement limit of an LVDT. According to eq. (7), the indentation creep on the straight-line region can be interpreted to be in a steady state. This result implies that a dislocation substructure corresponding to the individual stress level forms in the CV due to sufficient dynamic recovery during indentation creep. The detailed mechanism of this phenomenon will be reported elsewhere. From eq. (8), the slope of the straight lines allows us to determine the stress exponent n . The n value thus obtained varies distinctively

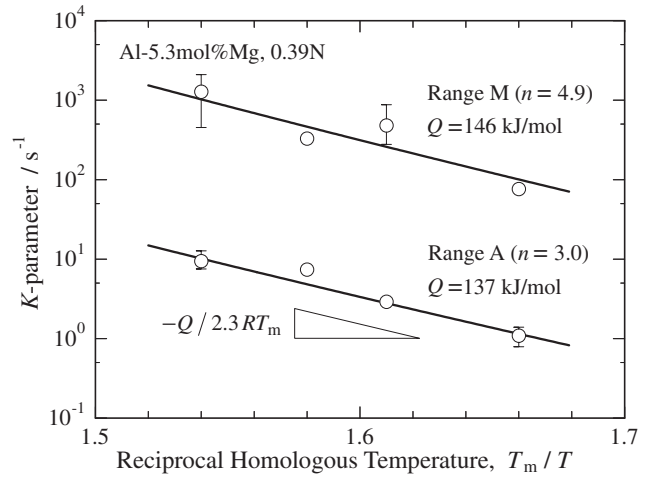
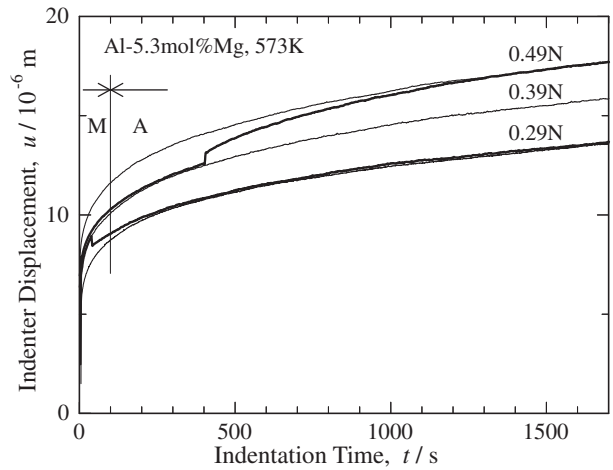

 Fig. 4 Temperature dependence of critical stress $\bar{\sigma}_c$.

 Fig. 5 Temperature dependence of critical indentation strain rate $\dot{\epsilon}_c$.

from 4.9 to 3.0 below a critical stress level $\bar{\sigma}_c$ and the corresponding indentation strain rate $\dot{\epsilon}_c$. Hereafter, the range of $\bar{\sigma}_m > \bar{\sigma}_c$ or $\dot{\epsilon}_{in} > \dot{\epsilon}_c$ is designated as range M ($n \cong 5$). In the case of $\bar{\sigma}_m < \bar{\sigma}_c$ or $\dot{\epsilon}_{in} < \dot{\epsilon}_c$, it is named range A ($n \cong 3$).

Figure 4 shows the temperature dependence of the critical stress level $\bar{\sigma}_c$, and that the value of $\bar{\sigma}_c$ decreases rapidly from 122 to 52 MPa for the temperature range of 546–590 K. For example, $\bar{\sigma}_c$ at 573 K is estimated to be 61 ± 6 MPa on average. As shown in the figure, our experimental results agree well with those obtained using conventional tensile creep tests in the literature.^{20–22}

Figure 5 shows the temperature dependence of the critical indentation strain rate $\dot{\epsilon}_c$, which corresponds to $\bar{\sigma}_c$. It is clear that $\dot{\epsilon}_c$ increases with increasing temperature. The activation energy obtained from Arrhenius plots of $\dot{\epsilon}_c$ is approximately 20 kJ/mol, which is rather small compared with the activation energy for the lattice diffusion of aluminum, 144 kJ/mol.²³

Figure 6 shows the Arrhenius plots of K -parameter obtained from analyzing the data lying on the straight lines in Fig. 3. Here, $K = \dot{u}u^{-1}(Eu^2/F)^n$ holds. The K values fall on two straight lines with different slopes. Equation (9)


 Fig. 6 Arrhenius plots of K -parameter, $K = \dot{u}u^{-1}(Eu^2/F)^n$, in ranges M ($n \cong 5$) and A ($n \cong 3$).

 Fig. 7 Results of indentation load-jump test. Thin lines represent ICCs with constant loads of 0.29 N, 0.39 N and 0.49 N at $T = 573$ K. Thick lines denote ICCs obtained with the abrupt change in indentation load from 0.39 N to 0.29 N or from 0.39 N to 0.49 N.

indicates that the slope of either straight line corresponds to $-Q/2.3RT_m$. The activation energy for creep thus obtained is $Q = 146$ kJ/mol in range M ($n = 4.9$), which agrees well with the value of 144 kJ/mol obtained for the lattice diffusion of pure aluminum.²³ In range A ($n = 3.0$), Q is 137 kJ/mol. This value is close to the activation energy for the mutual diffusion of an Al-Mg solid-solution alloy, 130 kJ/mol.²³

The above results suggest that the creep rate-controlling process changes from the climb motion to the glide motion of dislocations below a critical stress level, $\bar{\sigma}_c$, and the corresponding indentation strain rate $\dot{\epsilon}_c$ as indentation creep proceeds.

4.2 Load-jump test

Figure 7 shows the relationship between indenter displacement and indentation time. The ICCs (thin lines) show results obtained with constant loads of 0.29, 0.39 and 0.49 N at 573 K. One of the ICCs (thick lines) represents the case wherein load was abruptly decreased from 0.39 to 0.29 N in range M, and the other thick line denotes the case of load

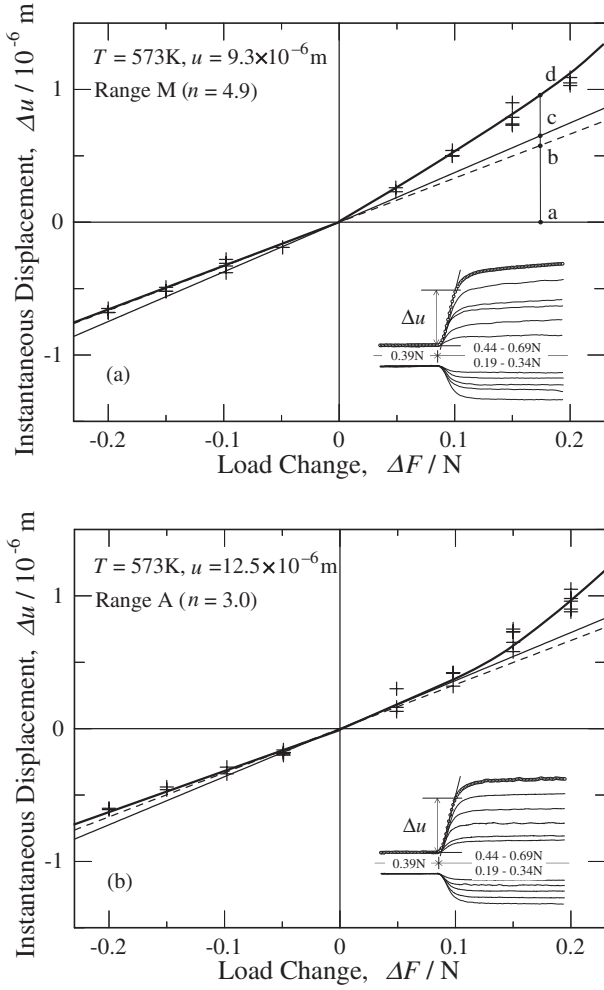


Fig. 8 Dependence of instantaneous displacement Δu on load increment ΔF in ranges M (a) and A (b). The inset shows a magnified view of the part of load jumping.

increase from 0.39 to 0.49 N in range A. The thick lines gradually approach the corresponding thin lines obtained by the constant-load tests after the transient stage. This result implies that the indenter velocity is uniquely determined with respect to the indenter displacement. This fact suggests that indentation strain rate is decided uniquely under certain representative stress, and this relationship does not depend on the load-application path. Figures 8(a) and 8(b) show the instantaneous displacement Δu as a function of load change ΔF . The abscissa is load increment ΔF , with positive values indicating increases and negative values indicating decreases. The ordinate is the instantaneous displacement Δu , with positive values indicating displacement in the indentation direction, and negative values indicating that in the opposite direction. In both figures, the negative values of Δu lie on a straight line. It is found that Δu is proportional to ΔF when load is abruptly decreased in ranges M and A. In contrast, when load is abruptly increased, the instantaneous deformation behavior of each stress range differs significantly. (a): When load is abruptly increased by approximately 0.05 N in range M, the Δu values lie above the straight line. (b): By contrast, with the abrupt load increase of $\Delta F \leq 0.10 \text{ N}$ in range A, the values of Δu still fall on the straight line.

However, the Δu values for $\Delta F > 0.10 \text{ N}$ lie above the straight line, similar to the case of (a).

5. Discussion

5.1 Determination of instantaneous plastic deformation in load-jump test

When load is abruptly increased during an indentation creep test, an instantaneous displacement Δu is detected via an LVDT. Δu may be derived from the elastic deformation of the testing machine and from both the elastic deformation and instantaneous plastic deformation of the specimen. For convenience, the elastic deformation and the instantaneous plastic deformation are represented by the symbols of ED and IPD, respectively. A method of dividing the measured Δu into two parts of ED and IPD is described in the following.

5.1.1 Compliance of microindenter

In the microindenter employed, a testing machine, an indenter tip and a specimen are connected in series as shown in Fig. 1(b). The compliance C of this mechanical system is given by^{24,25)}

$$C = C_m + \frac{1}{2aE_r} \sqrt{\frac{\pi}{A}}, \quad (10)$$

where C_m is the compliance of the load frame, which is obtained from the slope of an F - u curve in the case that a special jig is attached to the indenter setup. When $F = 0.39 \text{ N}$ and $T = 573 \text{ K}$, the corresponding C_m value is equal to $3.32 \times 10^{-6} \text{ m/N}$. The second term of eq. (10) represents the contact compliance between the indenter tip and the test surface, where E_r denotes the reduced elastic modulus, A denotes the projected contact area of an impression and a denotes unity for a conical indenter tip.²⁴⁾ The elastic contact theory provides the contact depth u_c of an indenter as follows.

$$u_c = u - C_m F - \xi(C - C_m)F \quad (11)$$

Here, $\xi = 0.72$ for conical indenter tips.²⁴⁾ When u_c is sufficiently larger than the radius of curvature of the indenter tip, the projected contact area of the impression A can be written as

$$A = 19.25[u - C_m F - 0.72(C - C_m)F]^2. \quad (12)$$

The reduced elastic modulus E_r is given by

$$\frac{1}{E_r} = \frac{1 - \nu_i^2}{E_i} + \frac{1 - \nu_s^2}{E_s}, \quad (13)$$

where E_i and E_s , and ν_i and ν_s are Young's modulus and Poisson's ratio of the indenter tip and the specimen, respectively, the values of which are $E_s = 58.00 \text{ GPa}$,¹⁹⁾ $\nu_s = 0.345$,²⁶⁾ $E_i = 1141 \text{ GPa}$ ²⁷⁾ and $\nu_i = 0.07$.²⁷⁾ From eqs. (10), (12) and (13), it follows that

$$\begin{aligned} & -3.56F(C - C_m)^2 + 4.95(u - C_m F)(C - C_m) \\ & - \frac{1 - \nu_i^2}{E_i} - \frac{1 - \nu_s^2}{E_s} = 0. \end{aligned} \quad (14)$$

In both ranges M and A, load-jump tests were performed under conditions of $F = 0.39 \text{ N}$, $u = 9.32 \times 10^{-6} \text{ m}$, and $F = 0.39 \text{ N}$, $u = 12.50 \times 10^{-6} \text{ m}$. When these values are substituted into eq. (14), it is found that the C values are $3.73 \times 10^{-6} \text{ m/N}$ in range M and $3.61 \times 10^{-6} \text{ m/N}$ in range

A. By multiplying the load increment ΔF by the compliance C , we can evaluate the amount of ED caused in the mechanical system for an abrupt change in load.

5.1.2 Determination of instantaneous plastic deformation

In Figs. 8(a) and 8(b), the slope of the thin straight lines allows us to determine the C of the mechanical system, and these lines represent the amount of ED caused in that system for an abrupt change in load. The slope of the dashed line denotes the compliance C_m of the load frame, and the value of $C_m \Delta F$ indicates the ED of its frame. Because the ED of diamond indenter tips is almost negligible, a-b corresponds to the ED of the testing machine and b-c that of the specimen. Accordingly, c-d indicates the IPD in the specimen for an abrupt increase in load. First, we discuss a case in which the indentation load F abruptly decreases. In both Figs. 8(a) and 8(b), it can be seen that the corresponding experimental data lie on the straight line with a slope of C . Therefore, the instantaneous displacement Δu for the abrupt decrease in load represents the ED of the testing machine and the specimen. On the other hand, when the F is abruptly increased, in range M of Fig. 8(a) IPD occurs even with a slight abrupt increase in load ($\Delta F < 0.05$ N). In range A of Fig. 8(b), with the abrupt load increase of $\Delta F \leq 0.10$ N, only ED takes place; when $\Delta F > 0.10$ – 0.15 N, ED as well as IPD occur simultaneously. Assuming that $F = 0.39 + (0.13$ – $0.15)$ N and $u = 12.5 \times 10^{-6}$ m, the stress level $\bar{\sigma}_{IP}$ at which the IPD occurs is 58–60 MPa. The measured $\bar{\sigma}_{IP}$ is fairly close to the critical stress $\bar{\sigma}_c$ (61 MPa) at a temperature of 573 K in Fig. 4. The above results can be explained as follows. Because thermal resistance to dislocation motion in range M ($\bar{\sigma}_m > \bar{\sigma}_c, n \cong 5$) does not exist or is almost negligible, most of dislocations can move at a high speed as if they are in free-flight motion in pure metals. As a result, IPD occurs even when there is only a slight abrupt increase in load. On the other hand, in range A ($\bar{\sigma}_m < \bar{\sigma}_c, n \cong 3$), thermal resistance exists and dislocations move viscously dragging the solute atmosphere. With the abrupt load increase of $\Delta F \leq 0.10$ N, because most of dislocations cannot move immediately due to their dragging resistance, only ED occurs. However, when the indentation load is abruptly increased so that $\bar{\sigma}_m$ almost exceeds $\bar{\sigma}_{IP} = 58$ – 60 MPa, many dislocations can break away from their solute atmosphere, and consequently, the occurrence of IPD is observed.

5.2 Theoretical investigation of critical stress and corresponding indentation strain rate

The creep rate-controlling process changes from the climb motion to the glide motion of dislocations in a solid-solution alloy at the critical stress level $\bar{\sigma}_c$ or the corresponding indentation strain rate $\dot{\epsilon}_c$. A set of equations regarding these material parameters is derived in the following. Figure 9 shows a schematic illustration of the relationship between the velocity v of an edge dislocation and its dragging resistance stress τ_R in the CV of a solid-solution alloy. At point A dislocations move at a high speed as if they are in free-flight motion in pure metals. When the dislocation velocity decreases from v_A at point A to v_B at point B as indentation creep proceeds, a solute atmosphere starts to form even around moving dislocations. Thereby, v_B suddenly decreases

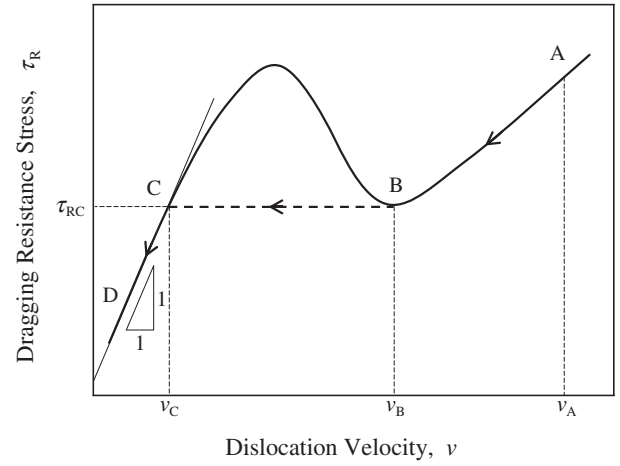


Fig. 9 Schematic illustration showing the relationship between dragging resistance stress τ_R and edge dislocation velocity v in a solid-solution alloy, both on logarithmic scales.

to v_C . Dislocations at point C are followed by a solute atmosphere that has a predetermined size of its own. In region C-D, dislocations move viscously dragging their solute atmosphere, and then v is proportional to τ_R .²⁸⁾ In accordance with computer simulations on dislocation motion in Al-Mg solid-solution alloys, point C almost corresponds to the point at which the $\tau_R - v$ relationship is no longer linear, and the velocity v_C at this point can be written as^{29,30)}

$$v_C = v_0 C_s^m \exp\left(-\frac{Q_v}{RT}\right), \quad (15)$$

where C_s denotes the molar concentration of solute atoms, $v_0 = 7.4 \times 10^5$ m/s, $m = 1.17$, $Q_v = 127$ kJ/mol. It is ascertained that the expression holds in the range of $C_s = 0.01$ – 0.05 . In general, the internal stress σ_i is given by

$$\sigma_i = \alpha b G M \sqrt{\rho}, \quad (16)$$

where α is a constant of 0.36,³¹⁾ b the magnitude of the Burgers vector (2.86×10^{-10} m), G the shear modulus, M the Taylor factor (3.06),³²⁾ and ρ the dislocation density. The rate of change in σ_i during creep deformation can be given as follows.

$$\frac{d\sigma_i}{dt} = \left(\frac{\partial\sigma_i}{\partial\varepsilon}\right)\dot{\varepsilon} - \left(-\frac{\partial\sigma_i}{\partial t}\right) \quad (17)$$

Here t denotes the time, ε denotes the plastic strain and $\dot{\varepsilon}$ denotes the plastic strain rate. The first term ($\partial\sigma_i/\partial\varepsilon$) represents a pure work-hardening rate without recovery effect, and the second term indicates a pure recovery-softening rate, which does not include the effects of work hardening. According to the dislocation theory,^{30,31)} eq. (17) can be approximately rewritten as

$$\frac{d\sigma_i}{dt} = \frac{\alpha^2 \beta b G^2 M^3}{4\sigma_i} \dot{\varepsilon} - \frac{\eta D}{2(\alpha b G M)^2} \sigma_i^3, \quad (18)$$

where β is the coefficient of dislocation multiplication, η the coefficient of recovery, and D denotes the diffusion coefficient.

Taking the steady state solution, *i.e.* $d\sigma_i/dt = 0$, $\dot{\varepsilon}$ is then given by

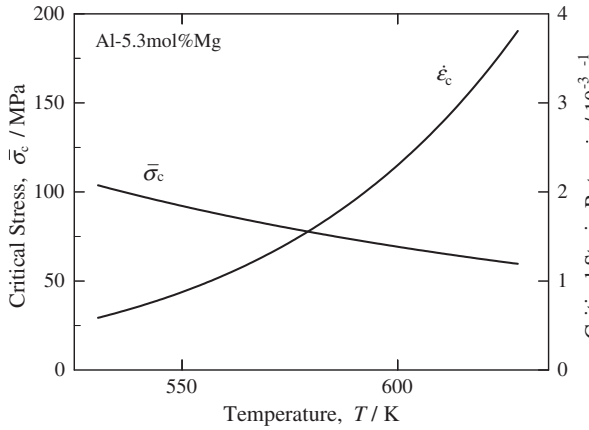


Fig. 10 Temperature dependences of $\bar{\sigma}_c$ and $\dot{\epsilon}_c$ obtained on the basis of the dislocation theory.

$$\dot{\epsilon} = \frac{2\eta D}{\alpha^4 \beta b^3 G^4 M^5} \sigma_i^4. \quad (19)$$

Also, $\dot{\epsilon}$ can be expressed as follows.

$$\dot{\epsilon} = \frac{2}{M} \rho b v \quad (20)$$

Assuming that most of the dislocations are in motion, the $\sigma_i - v$ relationship in a steady state is given from eqs. (16), (19) and (20) as

$$\sigma_i = \alpha b G M \sqrt{\frac{\beta}{\eta D}} v. \quad (21)$$

When the dragging resistance stress τ_R for dislocation motion is proportional to v ($v = B\tau_R$, where B is called the dislocation mobility), the deformation stress σ is given by the sum of σ_i and $M\tau_R$, that is

$$\sigma = \sigma_i + \frac{M}{B} v. \quad (22)$$

From eqs. (21) and (22), the relationship between the deformation stress $\bar{\sigma}_c$ and the dislocation velocity v_C at point C can be expressed by

$$\bar{\sigma}_c = \left(\alpha b G M \sqrt{\frac{\beta}{\eta D v_C}} + \frac{M}{B} \right) v_C. \quad (23)$$

From eqs. (4), (19) and (21), the indentation strain rate $\dot{\epsilon}_c$ corresponding to $\bar{\sigma}_c$ is given by

$$\dot{\epsilon}_c = \frac{6\beta b}{\eta D M} v_C^2. \quad (24)$$

Substituting eq. (15) into eqs. (23) and (24), the values of $\bar{\sigma}_c$ and $\dot{\epsilon}_c$ can be obtained.

Figure 10 shows the temperature dependence of $\bar{\sigma}_c$ and $\dot{\epsilon}_c$ evaluated using above equations. Table 2 lists material constants used in the calculation.^{23,29,31,33} As shown in the figure, $\bar{\sigma}_c$ decreases with increasing temperature, but $\dot{\epsilon}_c$ increases under the same condition. These computational results resemble the experimental results shown in Figs. 4 and 5. Therefore, the findings suggest that $\bar{\sigma}_c$ and $\dot{\epsilon}_c$

Table 2 Material constants used in evaluating $\bar{\sigma}_c$ and $\dot{\epsilon}_c$. G : the shear modulus, B : the dislocation mobility, D : the diffusion coefficient, β : the coefficient of dislocation multiplication, η : the coefficient of recovery.

T (K)	G (GPa)	B (m ³ /Ns)	D (m ² /s)	β (1/m)	η
573	21.0	4.73×10^{-15}	1.61×10^{-16}	9.61×10^6	98.3
623	20.0	4.22×10^{-14}	1.45×10^{-15}	2.86×10^6	87.3
673	19.4	2.87×10^{-13}	9.39×10^{-15}	9.54×10^5	77.6

correspond to their respective values below which the creep rate-controlling process changes from the climb motion to the glide motion of dislocations as indentation creep proceeds.

When β/η in eq. (24) is constant, the activation energy for $\dot{\epsilon}_c$ should be in close agreement with that for some diffusion; however, when β/η has some temperature dependence, they should not be in agreement. From the Arrhenius plot of theoretical values $\dot{\epsilon}_c$, we can determine the activation energy for $\dot{\epsilon}_c$, which is 62 kJ/mol. The value so obtained corresponds to approximately half of the activation energy for the mutual diffusion of this alloy. However, the activation energy for $\dot{\epsilon}_c$ obtained from our indentation creep tests is 20 kJ/mol. This discrepancy may be mainly due to the temperature dependence of β/η shown in Table 2; however, details of this discrepancy are still unknown.

On the other hand, we can theoretically predict from Fig. 9 that the stress level $\bar{\sigma}_{IP}$ at which the IPD is initiated in load-jump tests may be a little larger than the stress level $\bar{\sigma}_c$ below which the creep rate-controlling process changes from the climb motion to the glide motion of dislocations as indentation creep proceeds. However, the experimental values of $\bar{\sigma}_{IP}$ and $\bar{\sigma}_c$ are close to each other. The experimental result can be explained as follows. If there is not much difference between the maximum and minimum of τ_R values and there is a difference in the size of solution atmosphere around moving dislocations, it is likely that $\bar{\sigma}_c$ will be in close agreement with $\bar{\sigma}_{IP}$.

5.3 Transition of creep rate-controlling process

The experimental results on an Al-Mg solid-solution alloy show that the stress exponent n in range M ($\bar{\sigma}_m > \bar{\sigma}_c$ or $\dot{\epsilon}_{in} > \dot{\epsilon}_c$) is approximately 5, and the activation energy Q for creep is in close agreement with that for lattice diffusion of the pure aluminum matrix. Within this range, the thermal resistance to dislocation motion is almost negligible and dislocations can move at a high speed as if they are in free flight motion in the matrix. In range A ($\bar{\sigma}_m < \bar{\sigma}_c$ or $\dot{\epsilon}_{in} < \dot{\epsilon}_c$) $n \cong 3$, and the Q value is close to the activation energy for mutual diffusion of this alloy. In this range, the thermal resistance to dislocation motion exists and dislocations move viscously dragging the solute atmosphere. The above findings suggest that the indentation creep in range M is rate-controlled by a recovery process that depends on the climb motion of dislocations, similarly to creep deformation of pure metals with $n \cong 5$. On the other hand, the indentation creep in range A is rate-controlled by the glide motion of dislocations, which drag the solute atmosphere. Solid-solution alloys at high temperatures may deform plastically by five different deformation mechanisms.³⁴ The possible deformation mechanisms in the CV include dislocation climb rate-controlling creep (mechanism 1, $n = 5$), dislocation glide rate-control-

Table 3 Comparison between indentation creep test results and tensile creep test results.

Creep test method	Test materials	T (K)	$\bar{\sigma}$ (MPa)	Stress range	n	Q (kJ/mol)
Indentation (current study)	Al-5.3 mol% Mg alloy	546–590	23–151	M	4.9	146
				A	3.0	137
Tension (Murty <i>et al.</i> , 1972, 1973)	Al-5.5 mol% Mg alloy	573	5–250	M	4.9	140
				A	3.0	138
Tension (Yavari <i>et al.</i> , 1981, 1982)	Al-5.6 mol% Mg alloy	623	6–95	M	4.6	—
				A	3.0	149
Tension (Sato and Oikawa, 1988)	Al-1.1 mol% Mg alloy	570–640	2–50	M	4.3	137
				A	3.3	136

ling creep (mechanism 2, $n = 3$), Harper-Dorn creep (mechanism 3, $n = 1$), Nabarro-Herring creep (mechanism 4, $n = 1$), and Cobel creep (mechanism 5, $n = 1$). The two mechanisms 1 and 2 interact in a sequential manner, but the other mechanisms 3, 4 and 5 operate independently of each other. When all these mechanisms operate simultaneously, the measured indentation strain rate $\dot{\epsilon}_{in}$ can be expressed as

$$\dot{\epsilon}_{in} \cong 3\dot{\bar{\epsilon}} = 3\left(\frac{\dot{\epsilon}_1\dot{\epsilon}_2}{\dot{\epsilon}_1 + \dot{\epsilon}_2} + \dot{\epsilon}_3 + \dot{\epsilon}_4 + \dot{\epsilon}_5\right), \quad (25)$$

where $\dot{\epsilon}_i$ denotes the equivalent plastic strain rate for the i th deformation mechanism. Under the current experimental conditions ($\bar{\sigma}_m/E = 10^{-4}$ – 10^{-3} , $T/T_m = 0.60$ – 0.65), the values of $\dot{\epsilon}_3$, $\dot{\epsilon}_4$ and $\dot{\epsilon}_5$ are sufficiently smaller than $\dot{\epsilon}_1$ and $\dot{\epsilon}_2$.³⁵ Thus, eq. (25) can be reduced to

$$\dot{\epsilon}_{in} \cong 3\frac{\dot{\epsilon}_1\dot{\epsilon}_2}{\dot{\epsilon}_1 + \dot{\epsilon}_2}. \quad (26)$$

When the representative stress $\bar{\sigma}_m$ in the CV is larger than the critical stress level $\bar{\sigma}_c$ at which a solute atmosphere starts to form even around moving dislocations, it is anticipated that the solute atmosphere no longer hinders the motion of dislocations, which can move at a high speed. In this case, $\dot{\epsilon}_1 \ll \dot{\epsilon}_2$ holds and eq. (26) can be written as $\dot{\epsilon}_{in} \approx 3\dot{\epsilon}_1$. This means that indentation creep in range M is rate-controlled by some recovery process that depends on the climb motion of dislocations. In this case, it is known that the steady-state creep rate is typically proportional to the fifth power of applied stress, that is $\dot{\epsilon}_{in} \propto (\bar{\sigma}_m/E)^5$. On the other hand, when the glide velocity of the dislocations is of the order of the climb velocity due to solute atmosphere dragging, it follows that $\dot{\epsilon}_1 \approx 3\dot{\epsilon}_2$. Accordingly, the indentation creep in range A is rate-controlled by the viscous glide of dislocations, and it is known that $\dot{\epsilon}_{in} \propto (\bar{\sigma}_m/E)^3$ holds. The above results demonstrate that when $\bar{\sigma}_m$ decreases to $\bar{\sigma}_c$ or $\bar{\sigma}_{IP}$ as indentation creep proceeds, the creep rate-controlling process changes from the climb motion to the glide motion of dislocations and thus the stress exponent distinctively varies from 5 to 3.

5.4 Comparison with tensile creep test results

Table 3 lists our results and conventional creep test results found in the literature.^{20,22,36–38} In the current test, the stress exponent n is 4.9 and the activation energy Q for creep is 146 kJ/mol in range M; and $n = 3.0$ and $Q = 137$ kJ/mol in

range A. The results of tensile creep tests by Murty,²⁰ and Murty *et al.*³⁶ show that $n = 4.9$ and $Q = 140$ kJ/mol in range M, and $n = 3.0$ and $Q = 138$ kJ/mol in range A. Under similar conditions, the two testing methods give almost the same stress exponents and activation energies for creep. It is thus demonstrated that a self-similar indentation technique can be effectively used to extract material parameters equivalent to those obtained from conventional uniaxial creep tests in the dislocation creep regime.

6. Conclusions

Carefully designed self-similar indentation creep experiments were carried out to establish a robust and systematic method of extracting material parameters accurately from a testpiece as small as a rice grain. An Al-5.3 mol% Mg solid-solution alloy was chosen as a model material, and constant-load indentation tests and load-jump tests were performed at temperatures ranging from 546 to 590 K and at 573 K, respectively. The key results of this study can be summarized as follows.

- (1) When the representative stress $\bar{\sigma}_m$ and the indentation strain rate $\dot{\epsilon}_{in}$ in the underlying material decrease to the critical stress level $\bar{\sigma}_c$ and the corresponding indentation strain rate $\dot{\epsilon}_c$ as indentation creep proceeds, the stress exponent n for creep varies distinctively from 4.9 to 3.0.
- (2) The activation energy Q for creep in range M ($n \cong 5$, $\bar{\sigma}_m > \bar{\sigma}_c$ or $\dot{\epsilon}_{in} > \dot{\epsilon}_c$) is approximately equivalent to that for lattice diffusion of pure aluminum. The Q value in range A ($n \cong 3$, $\bar{\sigma}_m < \bar{\sigma}_c$ or $\dot{\epsilon}_{in} < \dot{\epsilon}_c$) is close to that for the mutual diffusion of this alloy.
- (3) With load-jump tests in range M, instantaneous plastic deformation (IPD) takes place evidently even with a slight abrupt increase in load. By contrast, the IPD does not occur in range A when load increment is within a certain value. However, the occurrence of IPD is observed when $\bar{\sigma}_m$ reaches $\bar{\sigma}_c$ or higher.
- (4) The measured $\bar{\sigma}_c$ and $\dot{\epsilon}_c$ correspond to their respective values below which the creep rate-controlling process changes from the climb motion to the glide motion of dislocations as indentation creep proceeds.
- (5) All the results thus obtained are in good agreement with those obtained from conventional tensile creep tests.
- (6) It is demonstrated that the self-similar indentation technique can be effectively used to extract material

parameters equivalent to those obtained from conventional uniaxial creep tests in the dislocation creep regime.

REFERENCES

- 1) A. C. Fischer-Cripps: *Nanoindentation*, (Springer-Verlag, New York, 2004).
- 2) *Microindentation Techniques in Materials Science and Engineering*, eds. P. J. Blau and B. R. Lawn (ASTM, Philadelphia, 1986).
- 3) T. O. Mulhearn and D. Tabor: *J. Inst. Metals* **89** (1960) 7–12.
- 4) W. B. Li, J. L. Henshall, R. M. Hooper and K. E. Easterling: *Acta Metall* **39** (1991) 3099–3110.
- 5) P. M. Sargent and M. F. Ashby: *Mater. Sci. Technol.* **8** (1992) 594–601.
- 6) O. Prakash: *Proc. The J. Weertman Symposium*, eds. by R. J. Arsenault *et al.*, (MMMS, PA, 1996) pp. 155–169.
- 7) B. N. Lucas and W. C. Oliver: *Metall. Mater. Trans. A* **30** (1999) 601–610.
- 8) M. Fujiwara and M. Otsuka: *J. Japan Inst. Metals* **63** (1999) 760–769.
- 9) M. Fujiwara and M. Otsuka: *Mater. Sci. Eng.* **A319–321** (2001) 929–933.
- 10) M. Fujiwara: *J. Japan Inst. Light Metals* **52** (2002) 282–290.
- 11) H. Takagi, M. Dao, M. Fujiwara and M. Otsuka: *Phil. Mag.* **83** (2003) 3959–3976.
- 12) M. Dao, H. Takagi, M. Fujiwara and M. Otsuka: *Mat. Res. Soc. Symp. Proc.* **795** (2004) 352–330.
- 13) R. Hill: *The Mathematical Theory of Plasticity*, (Oxford, Clarendon, 1983).
- 14) H. M. Pollock, D. Maugis and M. Barquins: *Microindentation Techniques in Materials Science and Engineering*, eds. P. J. Blau and B. R. Lawn (ASTM, Philadelphia, 1986) pp. 47–71.
- 15) Y. T. Cheng and C. M. Cheng: *Philos. Mag. Lett.* **81** (2001) 9–16.
- 16) D. Tabor: *The Hardness of Metals*, (Oxford: Clarendon, 1951).
- 17) K. L. Johnson: *J. Mechan. Phys. Solids* **18** (1970) 115–126.
- 18) A. Bolshakov and G. M. Pharr: *J. Mater. Res.* **13** (1998) 1049–1058.
- 19) K. Abe, Y. Tanji, H. Yoshinaga and S. Morozumi: *J. Japan Inst. Light Metals* **27** (1977) 279–281.
- 20) K. L. Murty: *Scr. Mater.* **7** (1973) 899–904.
- 21) H. Oikawa, K. Sugawara and S. Karashima: *Scr. Mater.* **10** (1976) 885–888.
- 22) P. Yavari and T. G. Langdon: *Acta metall.* **30** (1982) 2181–2196.
- 23) E. A. Brandes and G. B. Brook: *Smithells Metals Reference Book Butterworth-Heinemann*, (Oxford, Butterworth-Heinemann, 1992).
- 24) W. C. Oliver and G. M. Pharr: *J. Mater. Res.* **7** (1992) 1564–1583.
- 25) G. M. Pharr, W. C. Oliver and F. R. Brotzen: *J. Mater. Res.* **7** (1992) 613–617.
- 26) E. A. Brandes and G. B. Brook: *Smithells Metals Reference Book Butterworth-Heinemann*, (Oxford, Butterworth-Heinemann, 1992) pp. 15–2.
- 27) G. F. Cardinale, D. G. Howitt, K. F. McCarty, D. L. Medlin, P. B. Mirakarimi and N. R. Moody: *Diamond Relate. Mater.* **5** (1996) 1295–1302.
- 28) A. H. Cottrell: *Dislocations and Plastic Flow in Crystals*, (Oxford University Press, 1953).
- 29) H. Nakashima and H. Yoshinaga: *J. Japan Inst. Metals* **56** (1992) 254–261.
- 30) H. Miyagawa, T. Morikawa, T. Okazaki, H. Nakashima and H. Yoshinaga: *J. Japan Inst. Metals* **60** (1996) 367–376.
- 31) H. Miyagawa, H. Nakashima and H. Yoshinaga: *J. Japan Inst. Metals* **56** (1992) 531–540.
- 32) G. I. Taylor: *J. Inst. Metals* **62** (1938) 307–324.
- 33) J. L. Tallon and A. Wolfenden: *J. Phys. Chem. Solids* **40** (1979) 831–837.
- 34) H. J. Frost and M. F. Ashby: *Deformation-Mechanism Maps*, (Pergamon Press, Oxford, 1982).
- 35) F. A. Mohamed and T. G. Langdon: *Scr. metall.* **9** (1975) 137–140.
- 36) K. L. Murty, F. A. Mohamed and J. E. Dorn: *Acta metall.* **20** (1972) 1009–1018.
- 37) P. Yavari, F. A. Mohamed and T. G. Langdon: *Acta metall.* **29** (1981) 1495–1507.
- 38) H. Sato and H. Oikawa: *Scr. Mater.* **22** (1988) 87–92.